Available online at www.sciencedirect.com
SCIENCE DIRECT®
Journal of Catalysis 226 (2004) 197–209
JOURNAL OF CATALYSIS
www.elsevier.com/locate/jcat

Comparative isotope-aided investigation of electrochemical promotion and metal–support interactions
2. CO oxidation by $^{18}O_2$ on electropromoted Pt films deposited on YSZ and on nanodispersed Pt/YSZ catalysts

A. Katsaounis, Z. Nikopoulou, X.E. Verykios, C.G. Vayenas *

Department of Chemical Engineering, Caratheodory 1 St., University of Patras, GR-26504 Patras, Greece

Received 6 February 2004; revised 29 April 2004; accepted 6 May 2004

Abstract

The oxidation of CO by gaseous $^{18}O_2$ was investigated on electropromoted Pt films deposited on Y_2O_3-stabilized ZrO_2 (YSZ) and on nanodispersed Pt/YSZ catalysts under high vacuum and under atmospheric pressure conditions. For both catalyst systems and in both cases it was found that the temperature dependence of the catalytic oxidation rate can be correlated directly with the corresponding TPD spectra of $^{18}O_2$, $^{16}O^{18}O$, and $^{16}O_2$ and that lattice oxygen plays a key role in the oxidation reaction, acting both as a reactant and as a sacrificial promoter. For both systems the results confirm the sacrificial promoter model of electrochemical promotion and metal–support interactions with O^{2-}-conducting supports. This mechanism contains as limiting cases the promoted Langmuir–Hinshelwood and the Mars–van Krevelen mechanisms, which predominate at low and high temperatures, respectively.

1. Introduction

The electrochemical promotion (NEMCA effect) of catalytic reactions on porous conductive metal and metal oxide films deposited on ionic conductors has been investigated for more than 70 catalytic reactions [1–15]. The porous catalyst film is in contact with the ionically conducting support and electrical current or potential (±2 V) is applied between the catalyst film and a counter electrode also in contact with the ionically conductive support while monitoring the catalyst potential with respect to a reference electrode. The electrochemically induced change, Δr, in catalytic rate, r, can be up to 150 times larger than unpromoted catalytic rate r_0 and up to 3×10^5 times larger than the rate, I/nF, of oxygen ion supply to the catalyst.

It has been found via several surface spectroscopic and electrochemical techniques [16–19] that electrochemical promotion is due to electrochemically controlled (Faradaic) introduction of promoting ionic species ($O^{\delta-}$, $Na^{\delta+}$, H^+, etc.) to the catalytically active metal/gas interface and to the creation of a double layer at that interface [15,20,21]. The magnitude of electrochemical promotion is commonly described by two parameters: The apparent Faradaic efficiency, Λ, defined from

$$\Lambda = \Delta r/(I/nF), \tag{1}$$

where n is the charge of the electromigrating promoting species, and the rate enhancement ratio, ρ, defined from

$$\rho = r/r_0. \tag{2}$$

The promoting propensity of the electromigrating (backspillover) ionic species, j, is described by the promoter index, P_j, defined from

$$P_j = (\Delta r/r_0)/\Delta\theta_j, \tag{3}$$

where θ_j is the surface coverage of the promoting ion at the metal/gas interface.

The molecular mechanism of electrochemical promotion with O^{2-}-conducting or mixed O^{2-} electronic conducting supports has been found to be mechanistically equivalent

* Corresponding author.
E-mail address: cat@chemeng.upatras.gr (C.G. Vayenas).

0021-9517/$ – see front matter
doi:10.1016/j.jcat.2004.05.009

with that of metal–support interactions (MSI) with nanodispersed catalysts deposited on the same materials [22]. It involves migration (backspillover) of promoting $O^{\delta-}$ species (where δ is near 2) from the support to the metal/gas interface and continuous replenishment of O^{2-} in the support by gaseous O_2 at the counterelectrode (electrochemical promotion) or at another supported catalyst particle or directly at the support/gas interface (metal–support interactions). The promoting $O^{\delta-}$ species is distinct from normally chemisorbed gas-supplied atomic oxygen as shown by TPD, XPS, cyclic voltammetry [15–18], and very recently STM [19].

In the first part of the present study [23], we have used TPD of $^{18}O_2$ adsorbed on Pt films deposited on YSZ and on nanodispersed Pt/YSZ powder catalysts to investigate the nature of oxygen adsorption on these materials. In the present work we have used CO oxidation by $^{18}O_2$, as a model reaction, to elucidate the role of lattice and gas-supplied oxygen on these two types of catalytic materials and to test the sacrificial promoter model of electrochemical promotion and metal–support interactions.

The oxidation of CO on Pt is the most thoroughly studied catalytic reaction in surface science and catalysis with several comprehensive reviews [24,25]. Recent studies have focused on low-temperature CO oxidation on supported Pt/Al_2O_3 catalysts [26–28] and have shown that the low-temperature activity is largely due to the reaction of linearly bonded CO (LCO) with weakly adsorbed atomic oxygen (O_{wads}) [28]. In the first part of the present work [23] we have also identified via TPD a similar weakly bonded oxygen state on Pt/YSZ (termed β_1 state [23]) desorbing at temperatures 100–160 °C which appears to be of similar nature as the O_{wads} state [28] and similar weakly bonded states observed on Pt/Al_2O_3 [29] and $Pt–Rh/Al_2O_3$ [30] catalysts. We have found similar β_1 states for Pt/CeO_2, Pt/TiO_2, and $Pt–W^{6+}$-doped TiO_2 catalysts [31]. These states are quite important for the low-temperature catalytic activity of supported Pt catalysts.

The CO oxidation on Pt is also one of the first two reactions shown to exhibit the phenomenon of electrochemical promotion on Pt films deposited on YSZ [32]. The study was performed at atmospheric pressure and gave ρ values up to 3 and Λ values up to 1000 [32]. The rather modest ρ values measured for CO oxidation can today be rationalized on the basis of the not too dissimilar dipole moments of adsorbed CO and atomic O [33].

According to the sacrificial promoter mechanism of electrochemical promotion and metal–support interactions [14,21], tested here for the first time via the use of $^{18}O_2$, the observed catalytic rate modification, Δr, in electrochemical promotion or metal support interactions is due to the two roles played simultaneously by the migrating (backspillover) $O^{\delta-}$ species:

a. Its role as a (relatively short-lived) promoter, primarily via electrostatic repulsive and attractive interactions at the metal/gas interface (e.g., with O(a) and CO(a) respectively in the case of CO oxidation); and
b. Its role as a reactant (e.g., with CO in the present case). Several techniques have shown that $O^{\delta-}$ is more strongly bonded and less reactive than O(a) for oxidation reactions [14,16].

Thus, according to the sacrificial promoter mechanism, the observed rate increase, Δr, in the rate of CO oxidation during an electrochemical promotion experiment (where a positive (anodic) current I is applied and O^{2-} is supplied to the catalyst at a rate $I/2F$) consists of two terms:

a. A (large) increase in the rate of CO oxidation by gas-supplied oxygen, denoted by $r_{C^{16}O^{18}O}$ when $^{18}O_2$ is used as the gas-phase oxidant; and
b. A (smaller and limited by $I/2F$) increase in the rate of CO oxidation by support-supplied oxygen, denoted by $r_{C^{16}O_2}$ when the support contains ^{16}O.

The use of the $^{18}O_2$ as the gas-supplied oxidant enables one to directly examine the validity of this mechanism.

2. Experimental

The Pt/YSZ catalysts (electropromoted Pt film and nanodispersed Pt/YSZ powder) used in the present kinetic investigation are *the same* as those used for the $^{18}O_2$ TPD investigation in part 1 of this work [23].

The preparation and characterization of the model electrochemically promoted catalyst (Pt film deposited on YSZ) were presented in detail in part 1 of this work [23]. In brief, the porous Pt film which was deposited on an YSZ disk (Dynamic-Ceramic; diameter 19 mm; thickness 2 mm) had a mass of 3.15 mg, a superficial surface area of 1 cm^2, and a thickness of approximately 1.1 μm. Its true surface area, N_G, expressed in maximum reactive oxygen uptake, was 2.7×10^{-8} mol O (±30%) and its three-phase-boundary (tpb) length, again expressed as maximum reactive oxygen uptake, was 4.9×10^{-11} mol O [23] (Fig. 1).

The preparation and characterization of the supported nanodispersed Pt/YSZ catalyst (1% Pt/YSZ) were presented in detail in part 1 of this work [23]. The Pt surface area was 1.8×10^{-5} mol Pt/g catalyst which corresponds to a metal dispersion value of 0.35 (±20%).

2.1. Temperature-programmed reaction (TPR) of electropromoted Pt/YSZ film under HV conditions

The UHV system (base pressure 10^{-10} Torr after baking) equipped with a quadrupole mass spectrometer (Balzers QMG 420) and a Balzers leak valve gas inlet system has been described in part 1 of this work [23].

The TPR experiments of CO oxidation were carried out by continuously feeding the 0.25% $C^{16}O$–1% $^{18}O_2$ reactive

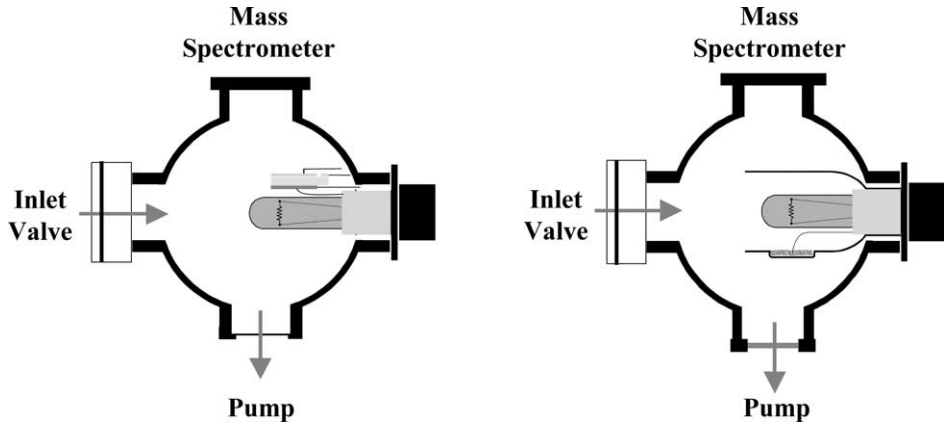

Fig. 1. Schematic of the UHV chamber and heating system used for TPD and TPR experiments with the Pt/film/YSZ disk sample with Au counter and reference electrodes (left) and with the 1% Pt/YSZ powder sample (right).

mixture into the vacuum system and maintaining the vacuum chamber at controlled total pressures of the order of 10^{-5} mbar. At a total pressure of 10^{-5} mbar the total gas flow rate fed to the vacuum system was 2.5×10^{-7} mol gas/s (0.35 cm^3 STP/min); i.e., the feed flow rate of $^{18}O_2$ was 2.5×10^{-9} mol $^{18}O_2$ and that of CO was 6.3×10^{-10} mol CO.

The Pt film temperature was increased linearly at a rate β (of the order of 0.5 °C/s) typically between 30 and 700 °C while monitoring the MS signals at AMU 28, 32, 34, 36, 44, and 46 for $C^{16}O$, $^{16}O_2$, $^{16}O^{18}O$, $^{18}O_2$, $C^{16}O_2$, and $C^{16}O^{18}O$, respectively. No significant signals at AMU 30 ($C^{18}O$) and 48 ($C^{18}O_2$) were measured. The above signals and concomitant rates of formation of $C^{16}O_2$ and $C^{16}O^{18}O$, as well as $^{16}O^{18}O$, were calibrated using standard CO_2 and O_2 calibration gases and converted into moles O per second signals by using the $^{16}O_2$ signal increase ($= I/4F$) generated upon imposing constant currents, I, between the Pt catalyst and the Au counterelectrode as described in detail in part 1 of this work [23]. Thus all feed flow rates and reaction rates could be expressed in moles per second.

The temperature-programmed reaction experiments of CO oxidation by $^{18}O_2$ were carried out in two modes: (a) under open-circuit conditions ($I = 0$), in which case the catalyst potential, U_{WR}, with respect to reference (R) electrode was also recorded during the TPR run; and (b) under constant applied potential U_{WR} (typically 1.2 V) in which case the current I and concomitant rate, $I/2F$, of O^{2-} supply to the Pt catalyst were also recorded during the TPR run.

In addition to the TPR runs, a series of *isothermal* galvanostatic (constant current) electrochemical promotion experiments was also carried out. In these transient experiments both the time evolution of the reaction rates ($r_{C^{16}O_2}$, $r_{C^{16}O^{18}O}$, $r_{^{16}O^{18}O}$) and of the catalyst potential U_{WR} could be recorded.

Constant currents or potentials were applied by using an AMEL 553 galvanostat-potentiostat.

2.2. Temperature-programmed reaction (TPR) of nanodispersed Pt/YSZ catalyst under HV conditions

The experiments were carried out in the same UHV system using the same feed composition (0.25% $C^{16}O$ + 1% $^{18}O_2$) and a total pressure of 2×10^{-6} mbar. Typically 140 mg of powder catalyst was placed in a quartz container with a thermocouple embedded in the powder and the powder temperature was varied linearly between 30 and 700 °C at a rate β of the order of 0.5 °C/s.

2.3. Temperature-programmed reaction with preadsorbed $^{18}O_2$ of nanodispersed Pt/YSZ catalyst under atmospheric pressure conditions

The Pt/YSZ powder sample (200 mg) was placed in the same atmospheric pressure cell used for the atmospheric pressure O_2 TPD investigation [23] and was first exposed to O_2 ($P_{^{18}O_2} = 2$ kPa at 70 °C for 60 min). Subsequently the cell was purged for 2 min with ultrapure He followed by a supply of 0.25% CO at atmospheric pressure (balance He) at 30 cc STP/min and simultaneous start of the TPR run with a heating rate $\beta = 1.5$ °C/s.

3. Results and discussion

3.1. CO oxidation by $^{18}O_2$ on Pt films deposited on YSZ

Fig. 2a shows the temperature dependence of the rates of $C^{16}O^{18}O$ and $C^{16}O_2$ formation under open-circuit conditions. The former rate is due to the reaction of CO with gas-supplied $^{18}O_2$; the latter is due to reaction of CO with ^{16}O originating from the YSZ lattice. In Fig. 2 and subsequent figures the rate of CO consumption was found to trace within experimental error the total rate of CO_2 formation and is thus not shown separately. Fig. 2a also shows the temperature dependence of the open-circuit catalyst potential, U_{WR},

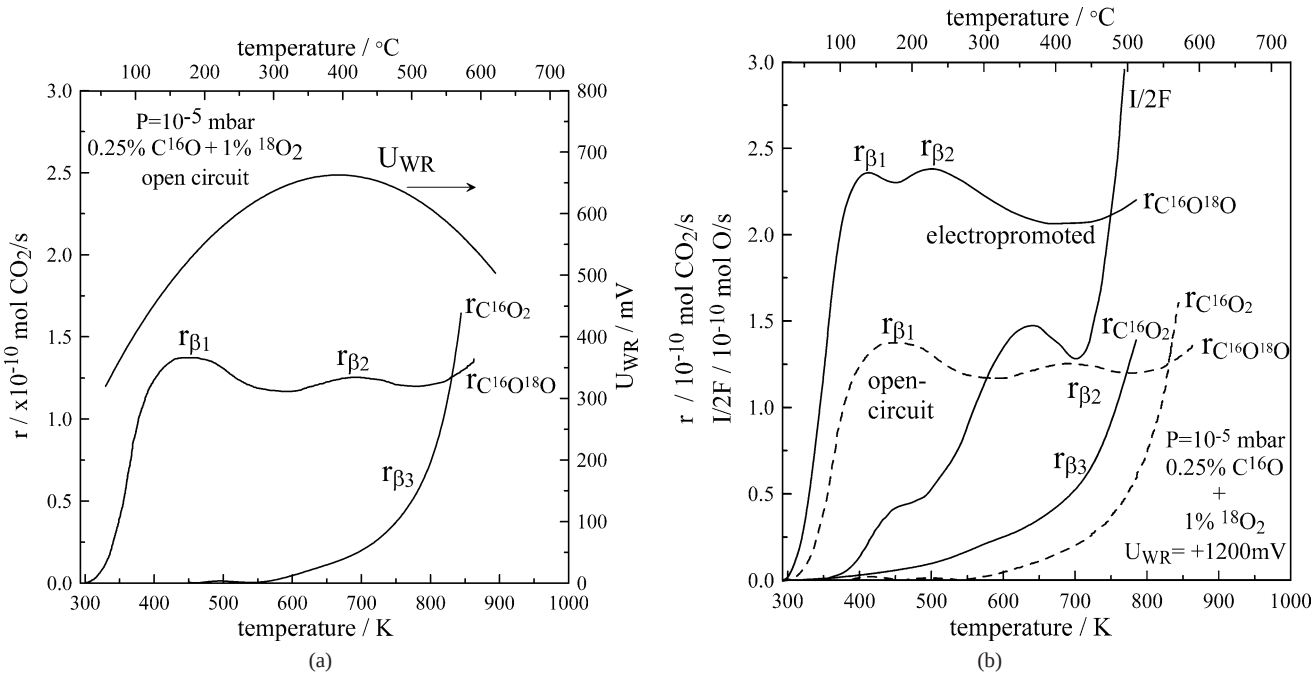

Fig. 2. (a) Pt film/YSZ: Temperature dependence of the rates of $C^{16}O^{18}O$ and $C^{16}O_2$ formation and of catalyst potential under open-circuit conditions. $P_{^{18}O_2} = 10^{-7}$ mbar and $P_{C^{16}O} = 0.25 \times 10^{-7}$ mbar. The heating rate was 0.5 °C/s. (b) Pt film/YSZ: Temperature dependence of the rates of $C^{16}O^{18}O$ and $C^{16}O_2$ formation and of oxygen ion supply rate $I/2F$ under electrochemical promotion conditions ($U_{WR} = 1.2$ V, solid curves) and under open-circuit ($I = 0$, broken curves). $P_{^{18}O_2} = 10^{-7}$ mbar and $P_{C^{16}O} = 0.25 \times 10^{-7}$ mbar. In both cases the heating rate was 0.5 °C/s.

which over wide ranges of temperature [14,34] is related to the catalyst work function, Φ, via

$$eU_{WR} = \Phi - \Phi_R, \tag{4}$$

where Φ_R is the work function of the reference (Au) electrode. Thus increasing U_{WR} denotes, in general, increasing Φ.

As shown in Fig. 2a, the rate of $C^{16}O^{18}O$ formation is already measurable at 50 °C and passes through two local maxima upon increasing temperature: one at 160 °C, the other at 420 °C. We will denote these two rate maxima as r_{β_1} and r_{β_2} because, as shown below, they can be directly related to the β_1 and β_2 oxygen adsorption states on the Pt/YSZ films, both of which are occupied by ^{18}O [23].

The rate of $C^{16}O_2$ formation is negligible below 250 °C and then increases exponentially with temperature with an apparent activation energy of 20 kcal/mol, which is very close to the literature value for the activation energy of O^{2-} conduction in YSZ [14]. It exceeds the rate of $C^{16}O^{18}O$ formation at 540 °C. Thus, above this temperature, the Mars–van Krevelen (MVK) mechanism of CO oxidation predominates over the Langmuir–Hinshelwood (LH) mechanism. We will denote the rate of $C^{16}O_2$ formation as r_{β_3} because it is directly related with the β_3 oxygen adsorption state of Pt/YSZ films and dispersed catalysts which is always occupied by lattice oxygen ^{16}O [23]. For the Pt/YSZ films the β_3 state is the only source of lattice oxygen, ^{16}O, for the formation of $C^{16}O_2$.

It is worth noting in Fig. 2a that the onset of U_{WR} (thus also Φ) decrease takes place at 420 °C, i.e., at the temperature where the rate maximum r_{β_2} appears. At this point r_{β_3} is already significant.

Fig. 2b compares the above open-circuit $r_{C^{16}O^{18}O}$ and $r_{C^{16}O_2}$ behavior (dashed curves) with that obtained under electrochemical promotion conditions ($U_{WR} = 1.2$ V, solid curves). The figure also shows the temperature dependence of the electrochemical rate, $I/2F$, of supply (backspillover) of O^{2-} from the YSZ support to the electropromoted Pt film. It must be noted that since the feed supply of CO and $^{18}O_2$ was 6.3×10^{-10} mol CO/s and 2.5×10^{-9} mol $^{18}O_2$/s, respectively, the maximum CO and $^{18}O_2$ conversions in Fig. 2 are on the order of 35 and 4%, respectively.

Fig. 2b has several noteworthy features:

a. Both the rate of supply of O^{2-}, $I/2F$, and the rate of $C^{16}O_2$ formation become measurable above 100 °C.
b. Both the $r_{C^{16}O_2}$ and the electrochemical promotion-induced rate increase $\Delta r_{C^{16}O_2}$ are always smaller than $I/2F$.
c. The electrochemical promotion-induced increase in the rate of $C^{16}O^{18}O$, $\Delta r_{C^{16}O^{18}O}$, is larger than $I/2F$ for temperatures below 310 °C (non-Faradaic rate enhancement).

As already noted, observations (b) and (c) form the basis of the sacrificial promoter concept [14,21], also discussed below.

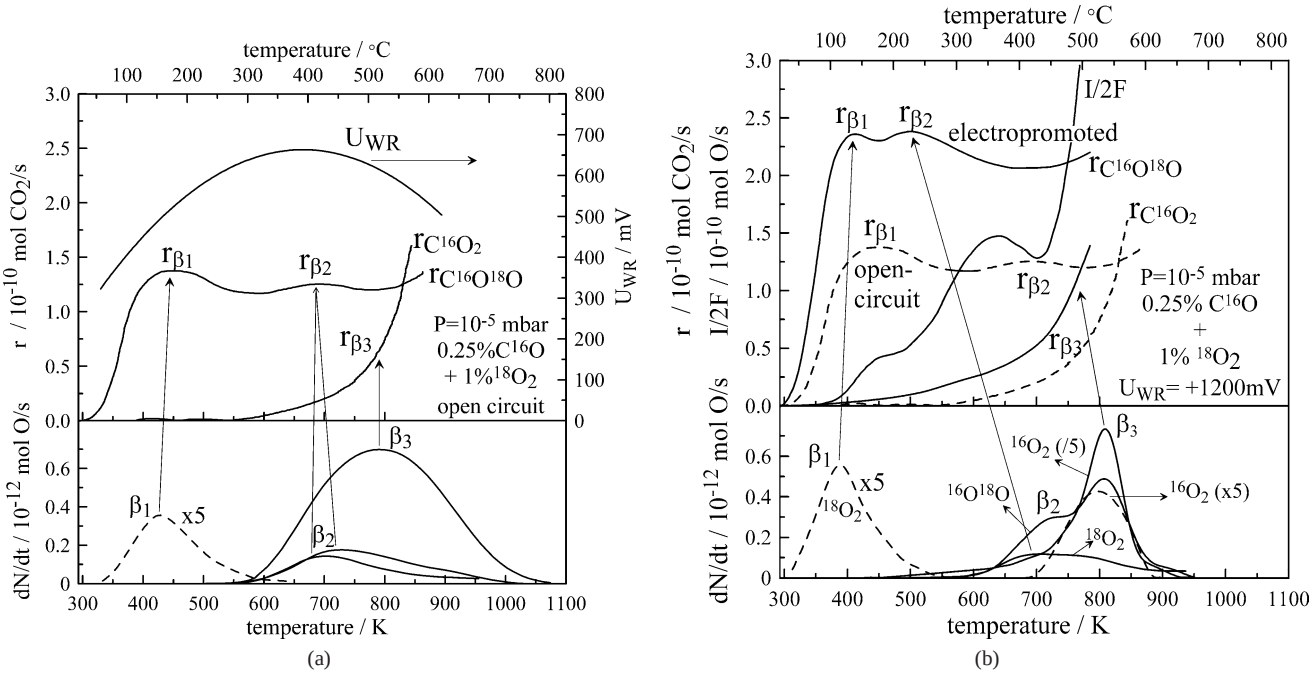

Fig. 3. (a) Pt film/YSZ: (top) Temperature dependence of the rates of $C^{16}O^{18}O$ and $C^{16}O_2$ formation and of catalyst potential under open-circuit conditions, $P_{^{18}O_2} = 10^{-7}$ mbar and $P_{C^{16}O} = 0.25 \times 10^{-7}$ mbar and (bottom) oxygen thermal desorption spectra after gaseous $^{18}O_2$ adsorption on the Pt film under open-circuit at 70 °C (broken line, $P_{^{18}O_2} = 10^{-7}$ mbar for 30 min) and at 275 °C (solid lines, $P_{^{18}O_2} = 10^{-6}$ mbar for 45 min) [23]. Heating rate 0.5 °C/s. (b) Pt film/YSZ: (top) Temperature dependence of the rates of $C^{16}O^{18}O$ and $C^{16}O_2$ formation and of oxygen ion supply rate $I/2F$ under electrochemical promotion conditions ($U_{WR} = 1.2$ V, solid curves) and under open-circuit ($I = 0$, broken curves), $P_{^{18}O_2} = 10^{-7}$ mbar and $P_{C^{16}O} = 0.25 \times 10^{-7}$ mbar, and (bottom) oxygen thermal desorption spectra after gaseous $^{18}O_2$ adsorption on the electropromoted Pt film at 70 °C and at 275 °C, $P_{^{18}O_2} = 10^{-6}$ mbar for 45 min followed by electrochemical $^{16}O^{2-}$ supply for 210 s with a constant current of +15 μA) [23]. Heating rate 0.5 °C/s.

d. The two local rate maxima in $r_{C^{16}O^{18}O}$ persist upon anodic potential application, but are shifted to significantly lower temperatures (120 vs 160 °C for r_{β_1} and 230 vs 420 °C for r_{β_2}). This temperature shift is noteworthy because it coincides with a concomitant decrease in the peak desorption TPD temperature of the β_1 and β_2 oxygen adsorption states as previously presented [23] and as also discussed below.
e. The current increase is not monotonic, indicating significant changes in the exchange current I_0 and anodic transfer coefficient α_a of the Butler–Volmer equation induced by changing coverages [14]. These oxygen coverage changes are discussed below in conjunction with the O_2 TPD spectra. It is noteworthy that the current I increases exponentially with temperature above 450 °C.

The close relationship between the rate maxima r_{β_1} and r_{β_2} and the corresponding oxygen adsorption states β_1 and β_2 on Pt films deposited on YSZ is shown in Fig. 3. Fig. 3a presents the *open-circuit r* vs T data of Fig. 2a together with the $^{18}O_2$ TPD spectra obtained on the *same* Pt/YSZ film for low ($T_{ads} = 70$ °C, dashed line) and high ($T_{ads} = 200$ °C, continuous line) $^{18}O_2$ adsorption temperatures. It can be seen that states β_1 and β_2, which are both occupied by gas-supplied $^{18}O_2$, can be assigned almost unambiguously to the corresponding rate maxima r_{β_1} and r_{β_2} of $C^{16}O^{18}O$ formation, while state β_3, which is always occupied by lattice oxygen ^{16}O clearly corresponds to the rate of $C^{16}O_2$ formation, r_{β_3}.

This assignment is further corroborated by examining the effect of positive potential (electropromoted film) on the rate maxima r_{β_1} and r_{β_2} and on the oxygen adsorption states β_1 and β_2 (Fig. 3b): As already discussed previously [23] the peak desorption temperatures of both states β_1 and β_2 are shifted to lower temperatures (115 vs 157 °C for state β_1 and 420 vs 450 °C for state β_2) due to lateral repulsive interactions between the adsorbed oxygen species on the electropromoted film (Ref. [23] and Fig. 3). As shown in Fig. 3b the rate maxima r_{β_1} and r_{β_2} are also shifted to lower temperatures (120 vs 160 °C for state β_1, 230 vs 420 °C for state β_2).

Consequently, in view of the above observations, the appearance of the two rate maxima in the $r_{C^{16}O^{18}O}$ vs T curves can be rationalized in a straightforward manner: The low T maximum (r_{β_1}) is due to the reaction of adsorbed CO with the oxygen adsorption state β_1 and the high T maximum (r_{β_2}) is due to the reaction of adsorbed CO with state β_2. It should be noted that the peak desorption temperature of CO is expected to be in the range 150–350 °C [26], i.e., between the peak desorption temperatures of the two oxygen adsorption states β_1 and β_2.

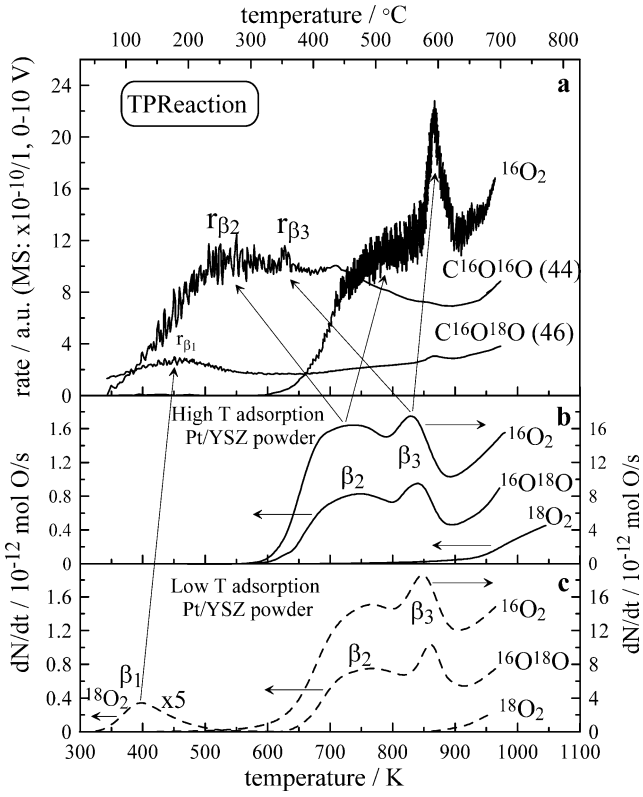

Fig. 4. Pt/YSZ powder under HV: (top) Temperature dependence of the rates of $C^{16}O^{18}O$ and $C^{16}O_2$ formation and of $^{16}O_2$ desorption using 140 mg of 1% Pt/YSZ nanodispersed catalyst, $P_{^{18}O_2} = 2 \times 10^{-8}$ mbar and $P_{C^{16}O} = 0.5 \times 10^{-8}$ mbar and (bottom) oxygen thermal desorption spectra after gaseous isotope oxygen dosing of 27 kL ($P_{^{18}O_2} = 10^{-7}$ mbar for 6 min) at 70 °C (broken lines) and at 200 °C (solid lines) [23]. Heating rate 0.5 °C/s.

3.2. CO oxidation by $^{18}O_2$ on nanodispersed Pt/YSZ catalysts

Fig. 4a shows the temperature dependence of the rates of $C^{16}O^{18}O$ and $C^{16}O_2$ formation, as well as the rate of $^{16}O_2$ desorption from the 1% Pt/YSZ nanodispersed catalyst for high (Fig. 4b) and low (Fig. 4c) adsorption temperature. It must be noted that the chaotic-looking small-amplitude variations in the rates of $C^{16}O_2$ and $C^{16}O^{18}O$ formation and $^{16}O_2$ desorption are not due to experimental noise, but rather the result of quasi-periodic self-sustained oscillations. There is a very rich literature on the oscillatory behavior of CO oxidation on both supported and unsupported Pt [24,32,35,36] and we will not discuss this subject further in the present work, as it is not of central importance here. Nevertheless it is interesting to note the oscillations in the rate of $^{16}O_2$ desorption (Fig. 4a) which, to the best of our knowledge, have not been reported before.

As shown in Fig. 4a, the rate of $C^{16}O^{18}O$ formation is generally smaller than the rate of $C^{16}O_2$ formation and passes through a single maximum, labeled r_{β_1}, at 170 °C. On the other hand, the rate of $C^{16}O_2$ formation is already measurable at 70 °C and passes through a wide maximum with increasing temperature where two smaller local rate maxima, labeled r_{β_2} and r_{β_3}, can be seen in the oscillatory region. We note that the small rate maximum labeled r_{β_3} is not an experimental artifact but has been observed in all (five) TPR runs we have performed, similar to that shown in Fig. 4a. As also shown in Fig. 4a the rate of $^{16}O_2$ desorption becomes measurable above 350 °C (i.e., the temperature where the maximum r_{β_3} appears) and exhibits a sharp maximum at 595 °C. This is the desorption temperature of the $^{16}O^{\delta-}$ backspillover-formed double layer present at the metal–gas interface [23] and coincides with the peak desorption temperature of state β_3 as shown in Fig. 4 and as discussed below.

In Figs. 4b and 4c, the TPR spectra of Fig. 4a are compared with the oxygen TPD spectra obtained on the *same* nanodispersed Pt/YSZ catalyst exposed to $^{18}O_2$.

One observes that the r_{β_1} maximum can be clearly correlated with the β_1 state ($T_P \approx 122$ °C) which is the only one occupied by gas-supplied $^{18}O_2$ on the nanodispersed Pt/YSZ catalyst (Ref. [23] and Fig. 4b) while the r_{β_2} and r_{β_3} maxima can be correlated with the β_2 and β_3 states which are both occupied by lattice oxygen, ^{16}O, on the nanodispersed catalyst. Note that the r_{β_2} maximum ($T = 230$ °C) occurs at the same temperature as in the case of the electropromoted Pt film (Fig. 3b).

One also notes that the $^{16}O_2$ TPD spectrum under reaction conditions (Fig. 4a) is very similar to the $^{16}O_2$ TPD spectrum in the absence of CO (Figs. 4b and 4c). Thus, ^{16}O not reacting with CO desorbs from the β_2 and β_3 states at only slightly higher temperatures than in absence of CO (Fig. 4). Note that the presence of adsorbed CO causes ^{16}O which in the absence of CO would desorb at 420 and 570 °C, respectively (states β_2 and β_3) to react with CO at 230 °C (r_{β_2}) and 350 °C (r_{β_3}), respectively (Fig. 4). This is quite reasonable since 350–400 °C is the highest temperature where CO remains on the Pt surface at significant coverages, as shown, e.g., by CO TPD spectra on Pt/Al_2O_3 [26]. Consequently the r_{β_2} and r_{β_3} peaks could not occur at any higher temperatures. It is interesting that both r_{β_2} and r_{β_3} in the TPR spectrum (Fig. 4a) appear approximately 200 °C lower than the corresponding β_2 and β_3 peak desorption temperatures in the ^{16}O TPD spectra (Figs. 4b and 4c).

Fig. 5a shows an atmospheric pressure TPR spectrum obtained with a 1% Pt/YSZ nanodispersed catalyst. The catalyst was first exposed to 2 kPa of $^{18}O_2$ for 60 min at 70 °C followed by 2 min purging in He at 70 °C and subsequent exposure to a flow of 30 cc STP/min containing $P_{CO} = 0.25$ kPa in He with a simultaneous increase in temperature with $\beta = 1.5$ °C/s. Figs. 5b and 5c show the corresponding $^{18}O_2$ [23] TPD spectra obtained with the same catalyst under atmospheric pressure conditions. Figs. 5a, 5b, and 5c show the same qualitative behavior as Figs. 4a, 4b, and 4c do; i.e., $r_{C^{16}O_2}$ is generally larger than $r_{C^{16}O^{18}O}$ and exhibits two maxima which correspond to the β_2 and β_3 adsorption states while $r_{C^{16}O^{18}O}$ exhibits one low-temperature maximum which corresponds to the β_1 state which is occupied by ^{18}O. It is interesting that the basic features of the

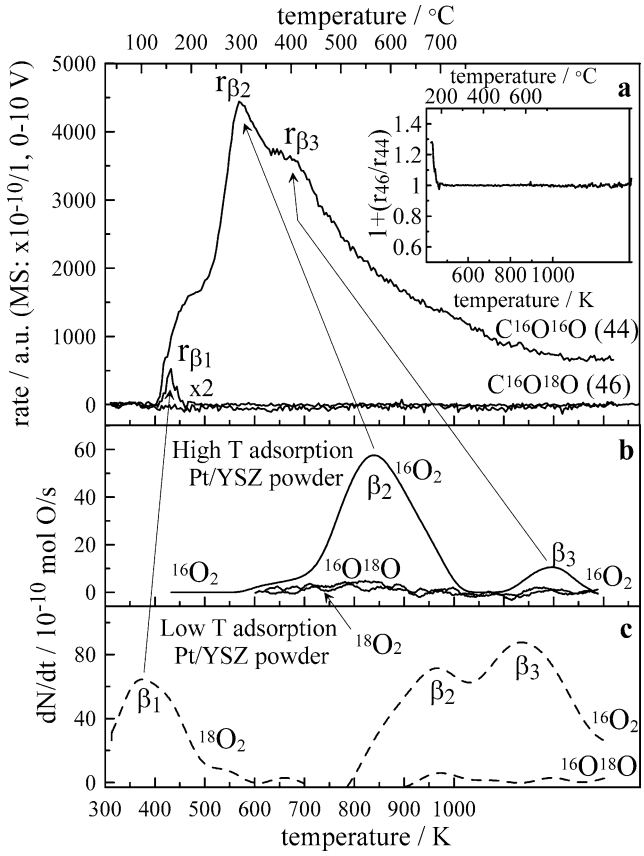

Fig. 5. Pt/YSZ powder under atmospheric pressure: (top) Temperature dependence of the rates of $C^{16}O^{18}O$ and $C^{16}O_2$ formation using 200 mg of 1% Pt/YSZ nanodispersed catalyst ($P_{^{18}O_2} = 20$ mbar for 60 min followed by reaction with $C^{16}O$ (0.25% in He, flow rate 30 cc/min); (bottom) atmospheric pressure and oxygen thermal desorption spectra after gaseous isotope oxygen dosing of ~54 kL ($P_{^{18}O_2} = 20$ mbar for 60 min) at 70 °C (broken lines) and at 200 °C (solid lines). Heating rate 1.5 °C/s.

CO oxidation mechanism remain the same as the pressure is increased by seven orders of magnitude between Fig. 4 and Fig. 5.

The area of the β_2 peak, which is occupied by ^{16}O, corresponds for the atmospheric pressure TPD (Fig. 5b) to 6×10^{-7} mol O and the combined $\beta_2 + \beta_3$ states (Fig. 5c) to 10^{-6} mol O. Since the total Pt surface area of the nanodispersed Pt/YSZ catalyst is 3.6×10^{-6} mol, the total atomic oxygen coverage is on the order of 0.25, in good agreement with the literature, for atmospheric pressure room temperature O_2 adsorption on Pt [14,15,24].

As already noted in part 1 of the present work [23], the only difference in the $^{18}O_2$ TPD spectra of electropromoted Pt films on YSZ and nanodispersed Pt/YSZ catalyst is the occupancy of the β_2 state: In the case of the films it is predominantly occupied by gas-supplied ^{18}O while in the case of the nanodispersed catalyst it is predominantly occupied by lattice oxygen, ^{16}O. This difference also manifests itself clearly in the temperature-programmed oxidation spectra (Figs. 3, 4, and 5).

In the case of the unpromoted and electropromoted film (Fig. 3) it is the rate of $C^{16}O^{18}O$ formation which exhibits *two* maxima, r_{β_1} and r_{β_2}, since both states β_1 and β_2 are occupied by ^{18}O, while in the case of the nanodispersed Pt/YSZ catalyst (Figs. 4 and 5) the rate of $C^{16}O^{18}O$ formation exhibits *one* maximum, r_{β_1}, and the rate of $C^{16}O_2$ formation exhibits *two* maxima, i.e., r_{β_2} and r_{β_3}, since in this case both states β_2 and β_3 are occupied by lattice oxygen ^{16}O.

In both cases (supported film and nanodispersed catalyst) the TPR spectra can be directly rationalized by the corresponding oxygen TPD spectra (Figs. 3b and 4). And in both cases lattice oxygen plays a key role in the CO oxidation kinetics acting both as a reactant and as a sacrificial promoter, as analyzed below.

3.3. Rationalization and prediction of transient and steady-state electrochemical promotion behavior

Fig. 6 is based on the data of Fig. 2b and presents some of the key results of the TPR investigation, by comparing the temperature dependence of (a) the rate, $I/2F$, of supply of O^{2-} to the Pt catalyst film, and (b) the observed increase, Δr_{total}, of the total rate of CO oxidation. Also shown (broken line) is the Faradaic efficiency Λ computed from Eq. (1). Since Δr in Eq. (1) has been computed using two different TPR experiments, i.e., one with applied potential ($U_{\text{WR}} = 1.2$ V), the other under open-circuit conditions ($I = 0$, U_{WR} varying as shown in Fig. 2), the thus computed Λ values (broken curve in Fig. 6) are estimates of the actual Faradaic efficiency, Λ, value expected to be observed under isothermal conditions in an isothermal galvanostatic or potentiostatic steady-state experiment.

Thus Fig. 6 can serve as a means of predicting the temperature ranges over which non-Faradaic ($\Lambda \gg 1$) or Faradaic ($\Lambda \leqslant 1$) behavior will be observed. The former behavior is predicted for $T < 310$ °C, the latter behavior ($\Lambda \leqslant 1$) for $T > 310$ °C. The points (filled circles) on Fig. 6 are actual isothermally measured Λ values from transient galvanostatic experiments of the type shown in Figs. 7 and 8 performed at practically the same total pressure ($P = 8 \times 10^{-6}$ mbar) as the TPR experiments (the open circle corresponds to a significantly lower pressure, $P = 2 \times 10^{-6}$ mbar). As shown in Fig. 6 there is very good agreement between the expected Λ values (dashed curve) and the actual Λ values measured isothermally (filled circles). This shows that during the TPR experiments (Figs. 2 to 5) the catalyst is near steady state regarding its catalytic activity.

Fig. 7 shows a low-temperature ($T = 225$ °C) galvanostatic experiment leading to non-Faradaic behavior ($\Lambda = 11.4$). As shown in Fig. 7 the rate of $C^{16}O_2$ formation increases or decreases very little with applied positive and negative current, respectively and these changes are Faradaic ($\Delta r_{C^{16}O_2} < (I/2F)$, thus $\Lambda_{C^{16}O_2} < 1$). On the other hand, the increase and decrease in the rate of $C^{16}O^{18}O$ formation are 11.4 and 9.6 times larger, respectively, than the rate, $|I/2F|$, of sup-

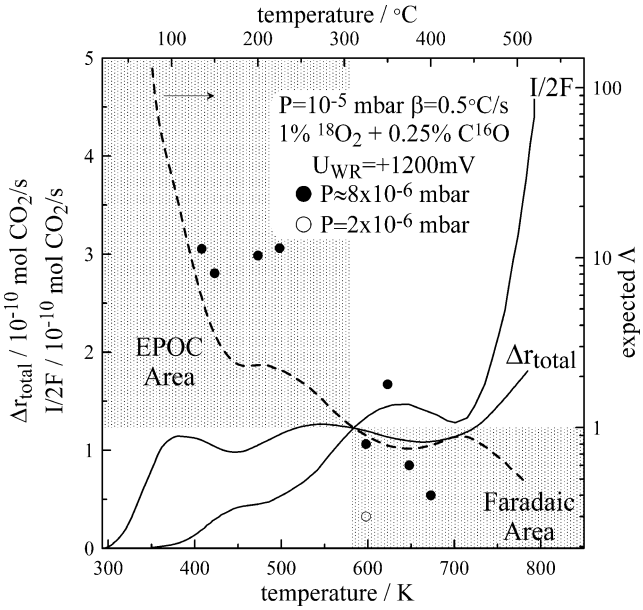

Fig. 6. Pt film/YSZ: Comparison of the temperature dependence of (a) the rate, $I/2F$, of supply of O^{2-} to the Pt catalyst film and (b) the observed increase, Δr_{total}, of the total rate of CO oxidation from the TPR curves of Fig. 2b. The broken curve shows the Faradaic efficient Λ computed from Eq. (1) and the filled circles show isothermally measured Λ values, at the same pressure $P = 8 \times 10^{-6}$ mbar, computed from Eq. (1). The open circle corresponds to $P = 2 \times 10^{-6}$ mbar and the same feed composition.

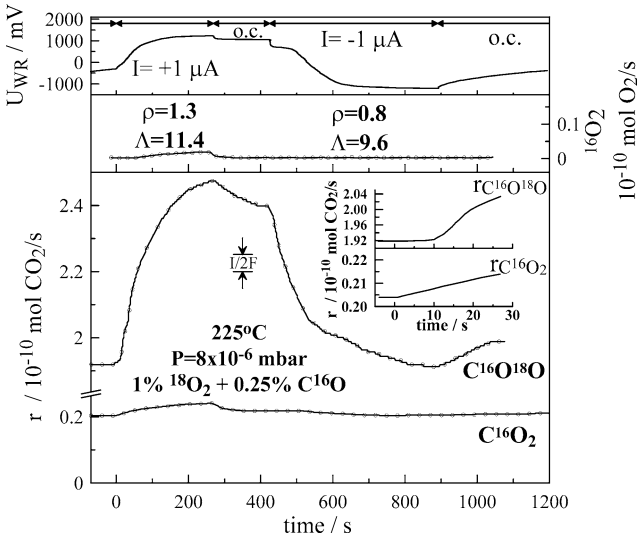

Fig. 7. Pt film/YSZ: Low-temperature ($T = 225\,^{\circ}\text{C}$) galvanostatic transient ($P_{^{18}O_2} = 8 \times 10^{-8}$ mbar, $P_{C^{16}O} = 2.5 \times 10^{-8}$ mbar) leading to non-Faradaic behavior ($\Lambda = 11.4$). Inset: Dynamic response of the two rates in the first few seconds after the current application.

ply or removal, respectively, of O^{2-} to or from the Pt catalyst film. Both observations confirm the sacrificial promoter ($^{16}O^{\delta-}$) mechanism of electrochemical promotion [14,21].

It should be noted in Fig. 7 that those $^{16}O^{2-}$ ions supplied to the catalyst which do not end up in $C^{16}O_2$ are desorbing to the gas phase. Under these conditions, YSZ is losing non-stoichiometric oxygen, O(YSZ) [14], but the loss is small in comparison with the total YSZ content of O (YSZ) [14,23].

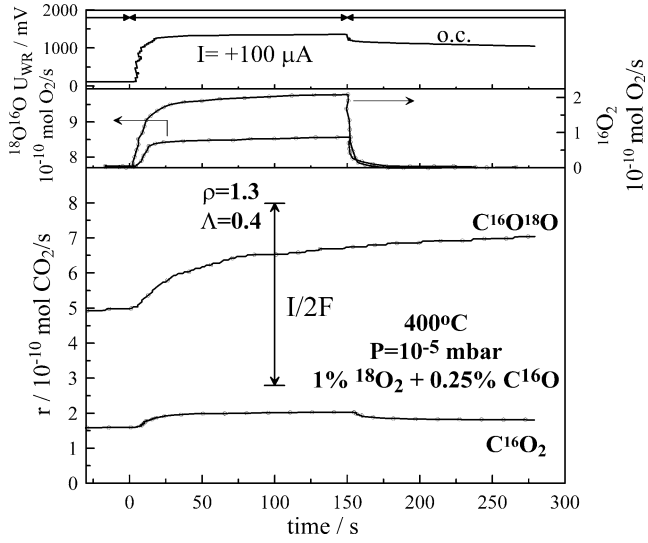

Fig. 8. Pt film/YSZ: High-temperature ($T = 400\,^{\circ}\text{C}$) galvanostatic experiment ($P_{^{18}O_2} = 10^{-7}$ mbar, $P_{C^{16}O} = 0.25 \times 10^{-7}$ mbar) leading to Faradaic behavior ($\Lambda = 0.4$).

One interesting aspect of Fig. 7, shown in the inset, is that upon current application the start of the increase in $r_{C^{16}O_2}$ is almost instantaneous, while the increase in $r_{C^{16}O^{18}O}$ follows a few (∼10) seconds later. This observation is also consistent with the sacrificial promoter mechanism of electrochemical promotion and with the formation of a diffuse propagation front of $^{16}O^{\delta-}$ which gradually moves on the catalyst–electrode surface, as experimentally observed via PEEM by Janek and co-workers [37]. The surface diffusion coefficient, D_S, of $^{16}O^{\delta-}$ can be estimated from the observed speed of propagation of such fronts but also, in principle, from the time lag observed between the $r_{C^{16}O_2}$ and the $r_{C^{16}O^{18}O}$ transients in the inset of Fig. 7. To this end one would have to fit these transients by the time-dependent version of the steady-state $^{16}O^{\delta-}$ reaction–diffusion models recently developed to describe the effect of catalyst–electrode thickness on the electrochemical promotion parameters ρ and Λ [38]. Such a moving $^{16}O^{\delta-}$ diffusion front has at a time τ after current application a finite thickness, L, given by $L = (D_S\tau)^{1/2}$. Behind this front the catalyst surface is in the fully electropromoted state, while in front of the front the surface is still at its unpromoted state. Thus a rough estimate of L and thus D_S can be obtained as follows.

As shown in the inset of Fig. 7 at $\tau = 10$ s where $\Delta r_{C^{16}O^{18}O}$ is still practically zero, the $\Delta r_{C^{16}O_2}$ value is 4×10^{-13} mol/s, i.e., has reached 7.5% of its final steady-state value of 5.3×10^{-12} mol/s. Assuming uniform initial surface concentration of CO, this implies that the front part of the diffusion front has propagated roughly 0.08 μm, since 1.1 μm is the total catalyst film thickness. Thus from $D_S = L^2/\tau$ one estimates $D_S = 6.4 \times 10^{-12}$ cm^2/s at 225 °C which is a reasonable value [14], corresponding to that extracted from the results of Lewis and Gomer [39] at 350 °C for O on Pt(111) and Pt(110) [14,39].

Fig. 8 shows a high-temperature ($T = 400\,^{\circ}C$) galvanostatic transient leading to Faradaic behavior ($\Lambda = 0.4$) and nearly complete CO conversion. Under these conditions most of the electrochemically supplied $^{16}O^{2-}$ desorbs as $^{16}O_2$ and thus the coverage of $^{16}O^{\delta-}$ remains low on the catalyst surface. Since the coverage of ^{18}O is also low due to the high temperature, the repulsive lateral interactions between $^{16}O^{\delta-}$ (i.e., state β_3) and ^{18}O (states β_1 and β_2) are much less pronounced [14,23]. Since these repulsive electrostatic interactions are one of the key factors leading to electrochemical promotion [14,40,41], no NEMCA behavior is observed ($\Lambda < 1$). Nevertheless it is interesting to observe in Fig. 8 that not only $r_{C^{16}O_2}$ but also $r_{C^{16}O^{18}O}$ increases during the galvanostatic transient; i.e., the promotional role of $^{16}O^{\delta-}$ supply and concomitant potential (Fig. 8) and work function increase are still evident, even though Λ remains below unity. Of course, the small Λ value is also dictated in the experiment by the near-complete CO conversion reached after current application.

It should be noted in Fig. 8, but also in Fig. 7, that upon current interruption the catalyst potential U_{WR} starts returning very slowly toward its initial value and application of a negative current (Fig. 7) is necessary to accelerate the process. This very slow return reflects the very slow reaction of the $^{16}O^{\delta-}$ species with the low-pressure CO in the vacuum system and is not so pronounced in atmospheric pressure electrochemical promotion studies where $^{16}O^{\delta-}$ is scavenged must faster due to the much higher pressure of the oxidizable reactant (e.g., CO) [14].

More quantitatively and using the measured Pt catalyst-film reactive oxygen uptake (2.7×10^{-8} mol O) one computes from the $r_{C^{16}O_2}$ values in Figs. 7 and 8 (0.2×10^{-10} mol ^{16}O/s and 1.6×10^{-10} mol ^{16}O/s, respectively) that the corresponding TOF values for $^{16}O^{\delta-}$ reaction with CO are 7.4×10^{-4} and 5.9×10^{-3} s^{-1}, respectively. Consequently the time required for $^{16}O_2$ removal from the catalyst surface upon current interruption is of the order of 1350 s (Fig. 7) and 170 s (Fig. 8), respectively, provided no additional ^{16}O migrates to the catalyst surface from the YSZ support. The latter is clearly a reasonable assumption at $T = 225\,^{\circ}C$ (Fig. 7), where indeed $r_{C^{16}O_2}$ starts decaying upon current interruption with a time constant of the order of 10^3 s, but, as expected [23], is clearly not a valid assumption at $400\,^{\circ}C$ (Fig. 8), where $r_{C^{16}O_2}$ decays much slower since, as already discussed [23], at these temperatures $^{16}O^{\delta-}$ is continuously replenished by $^{16}O^{2-}$ from the YSZ support and Pt film/YSZ catalyst exhibits, via exactly this $^{16}O^{2-}$ backspillover mechanism, a metal–support interaction [14,23].

3.4. Validation of the sacrificial promoter mechanism of electrochemical promotion and metal–support interactions

The present results enable one to validate the sacrificial promoter mechanism of electrochemical promotion and metal–support interactions. According to this mechanism

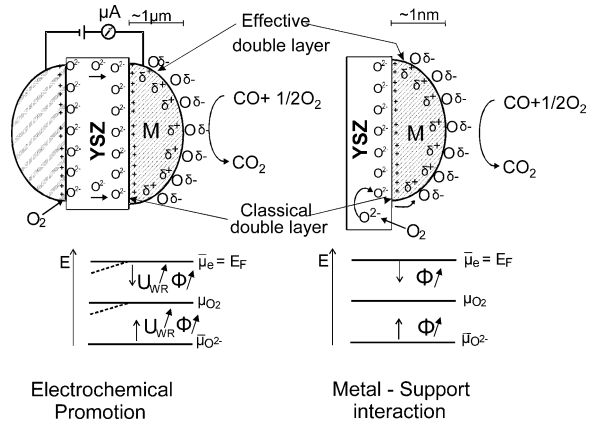

Fig. 9. Sacrificial promoter model of electrochemical promotion (left) and of metal support interactions (right): Schematic of a metal grain (μm) in a metal catalyst film deposited on YSZ under electrochemical promotion conditions (left) and of metal nanoparticles (∼nm) deposited on a porous YSZ support (right) showing the locations of the classical double layers formed at the metal/support interface and of the effective double layers formed at the metal/gas interface. The energy diagrams (bottom) indicate schematically the spatial constancy of the Fermi level E_F (or electrochemical potential $\bar{\mu}_e$) of electrons, of the chemical potential of oxygen and of the electrochemical potential of O^{2-}. Note that under electrical bias application (left) $\bar{\mu}_{O^{2-}}$ remains spatially constant but $\bar{\mu}_e$ and μ_{O_2} both bend in the solid electrolyte support (dashed lines). The Fermi level $\bar{\mu}_e$ of the metal can be affected by varying U_{WR} (left) or by varying via doping the Fermi level of the support (right). Oxygen ions migrate from the YSZ to the metal/gas interface via the three-phase boundaries and are replenished in YSZ by gaseous O_2.

(Fig. 9) promoting $^{16}O^{\delta-}$ ions migrate continuously from the support to the metal/gas interface, where they perform two functions:

a. They promote the catalytic reaction between the oxidable species (e.g., CO) and adsorbed ^{18}O originating from the gas phase (β_1 state and, in the case of Pt films, β_2 state). This results mainly from the increase in work function Φ and concomitant repulsive lateral electrostatic interactions between $^{16}O^{\delta-}$ and adsorbed ^{18}O, although the lateral interactions between $^{16}O^{\delta-}$ and coadsorbed CO also play a role [14,33,40,41].
b. They react with the oxidizable species (e.g., CO) with a rate which is Λ times smaller than the (promoted) rate of CO with ^{18}O [14]. In the limit $\Lambda = 1$ one has electrocatalysis, while in the limit $\Lambda \to \infty$ one has classical promotion with "infinite" lifetime of the promoting species on the catalyst surface.

Thus according to the sacrificial promoter mechanism, an O^{2-} arriving from the solid electrolyte support to the three-phase boundaries metal–gas–solid electrolyte (Fig. 9) has three possibilities:

a. Desorption as $^{16}O_2$,

$$^{16}O^{2-} \to \tfrac{1}{2}{}^{16}O_2(g) + 2e^-; \tag{5}$$

b. Reaction with adsorbed CO forming $C^{16}O_2$,

$$^{16}O^{2-} + C^{16}O \rightarrow C^{16}O_2(g) + 2e^-; \quad (6)$$

c. Migration (diffusion, backspillover) at the metal/gas interface as a surface dipole,

$$^{16}O^{2-} \rightarrow \left[^{16}O^{\delta-}\text{–}\delta^+\right] + 2e^-. \quad (7)$$

This surface anionic species promotes the rate of CO oxidation with coadsorbed ^{18}O and eventually can either desorb as $^{16}O_2$ or $^{16}O^{18}O$ or react with CO to form $C^{16}O_2$.

$$\left[^{16}O^{\delta-}\text{–}\delta^+\right] + C^{16}O \rightarrow C^{16}O_2. \quad (8)$$

Consequently each $^{16}O^{2-}$ arriving at the tpb will eventually either form $^{16}O_2$ or $^{16}O^{18}O$ or $C^{16}O_2$:

$$^{16}O^{2-} \overset{r_{^{16}O_2}}{\rightarrow} \tfrac{1}{2}\,^{16}O_2(g) + 2e^-, \quad (9)$$

$$^{16}O^{2-} + {}^{18}O(ad) \overset{r_{^{16}O^{18}O}}{\rightarrow} {}^{16}O^{18}O(g) + 2e^-, \quad (10)$$

$$^{16}O^{2-} + CO \overset{r_{C^{16}O_2}}{\rightarrow} C^{16}O_2(g) + 2e^-. \quad (11)$$

It follows from Faraday's law that

$$\Delta r_{C^{16}O_2} = S_p(I/2F), \quad (12)$$

$$2\Delta r_{^{16}O_2} + \Delta r_{^{16}O^{18}O} = (1 - S_p)(I/2F), \quad (13)$$

where the "promoter selectivity" parameter S_p, defined from the above equations, takes values between 0 and 1.

From Eq. (1) and taking into account that

$$\Delta r_{CO_2,\text{total}} = \Delta r_{C^{16}O^{18}O} + \Delta r_{C^{16}O_2}, \quad (14)$$

one obtains

$$\Lambda = \frac{\Delta r_{CO_2,\text{total}}}{I/2F} = \frac{\Delta r_{C^{16}O^{18}O} + \Delta r_{C^{16}O_2}}{\Delta r_{C^{16}O_2}} S_p; \quad (15)$$

i.e.,

$$\Lambda = S_p\left(1 + \frac{\Delta r_{C^{16}O^{18}O}}{\Delta r_{C^{16}O_2}}\right). \quad (16)$$

Consequently by plotting Λ $(= \Delta r_{CO_2,\text{total}}/(I/2F))$ vs $1 + \Delta r_{C^{16}O^{18}O}/\Delta r_{C^{16}O_2}$ one can examine the validity of the sacrificial promoter concept by examining if S_p remains between 0 and 1. This is indeed confirmed in Fig. 10. It can also be seen that at temperatures below 300 °C (points 6–9) (where Λ is above unity as anticipated from Fig. 6 and as shown in Fig. 10), S_p is close to unity and there is excellent agreement between the experiment and the limiting case of Eq. (16) obtained with S_p values of unity:

$$\Lambda \approx 1 + \frac{\Delta r_{C^{16}O^{18}O}}{\Delta r_{C^{16}O_2}}. \quad (17)$$

Note that in the case of large Λ and ρ values Eq. (17) further reduces to

$$\Lambda \approx 1 + \frac{r_{C^{16}O^{18}O}}{r_{C^{16}O_2}} \approx \frac{r_{C^{16}O^{18}O}}{r_{C^{16}O_2}}, \quad (18)$$

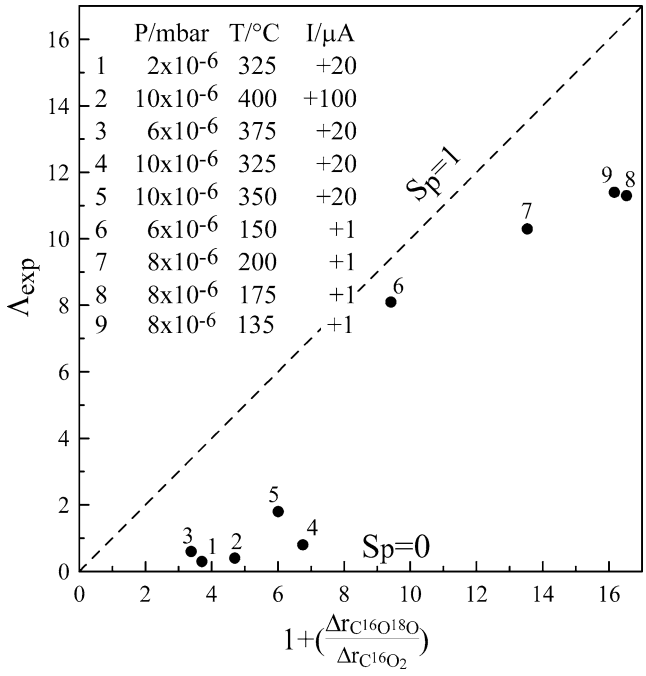

Fig. 10. Pt film/YSZ: Validation of the sacrificial promoter concept by plotting Λ $(= \Delta r_{CO_2,\text{total}}/(I/2F))$ vs $1 + \Delta r_{C^{16}O^{18}O}/\Delta r_{C^{16}O_2}$ and confirming that S_p is bounded between 0 and 1. $P_{^{18}O_2} = 8 \times 10^{-8}$ mbar, $P_{C^{16}O} = 0.25 \times 10^{-8}$ mbar.

and thus according to the sacrificial promoter mechanism in this limit the apparent Faradaic efficiency Λ expresses the ratio of the reaction rates of adsorbed ^{18}O and $^{16}O^{\delta-}$ with the oxidizable species (i.e., CO) or the ratio of the lifetimes of $^{16}O^{\delta-}$ and ^{18}O on the catalyst surface [14].

To the extent that the sacrificial promoter mechanism is valid, Eq. (18) can also be used to estimate the magnitude of Λ for supported catalysts where the rate, $I/2F$, of promoting $^{16}O^{\delta-}$ supply to the catalyst surface is not directly measurable.

Consequently the use of isotopic oxygen $^{18}O_2$ as the gas-phase oxidant enables one to directly examine the validity of the sacrificial promoter mechanism of electropromoted catalysts by examining the validity of Eq. (16) or Eq. (17) in conjunction with

$$\Delta r_{C^{16}O_2} \leqslant I/2F \quad (19)$$

or, more precisely, with

$$\Delta r_{C^{16}O_2} + 2\Delta r_{^{16}O_2} + \Delta r_{^{16}O^{18}O} = I/2F, \quad (20)$$

where each of the Δr terms is nonnegative.

At higher temperatures where $^{16}O_2$ desorption is favoured vs $^{16}O^{\delta-}$ reaction with CO, the sacrificial promoter mechanism remains operative with $S_p < 1$. Fig. 11 shows the temperature dependence of S_p which, as expected, decreases significantly with increasing T. This is because the activation energy for $^{16}O_2$ desorption is much higher than the activation energy for reaction of ^{16}O with CO. The $\ln S_p$ vs $1/T$ plot (Fig. 11) gives an apparent ΔH value of 21 kcal/mol in

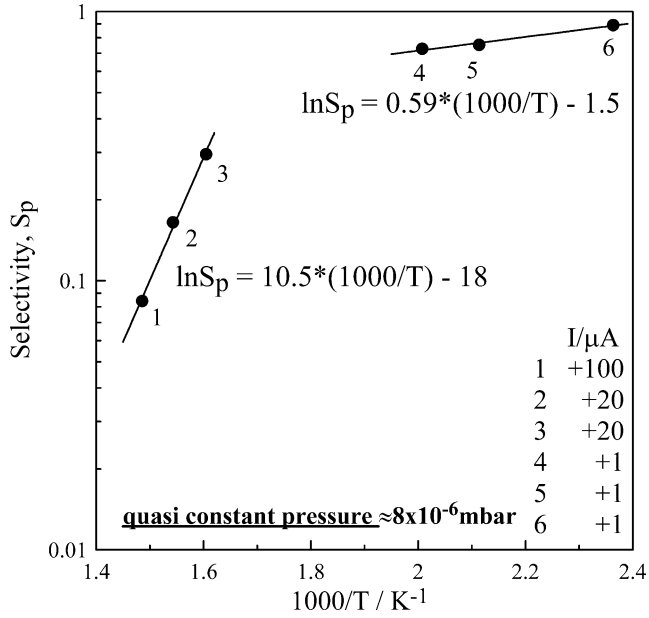

Fig. 11. Pt film/YSZ: Temperature dependence of S_p for various applied currents and quasi-constant pressure of 8×10^{-6} mbar. $P_{^{18}O_2} = 8 \times 10^{-8}$ mbar, $P_{C^{16}O} = 0.25 \times 10^{-8}$ mbar.

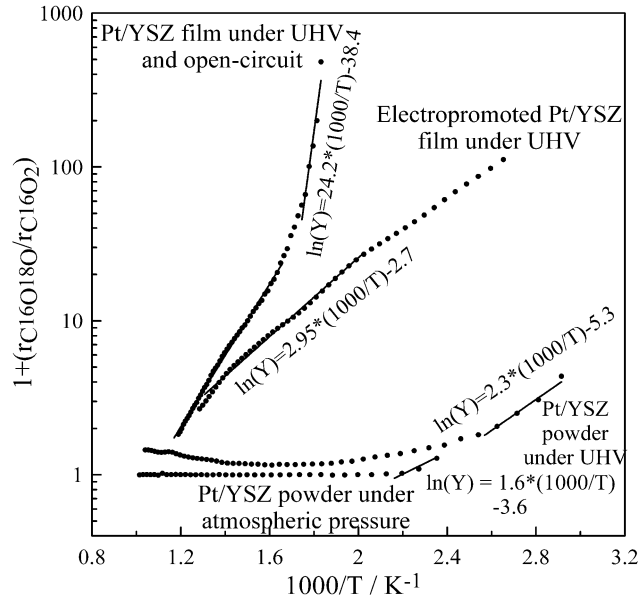

Fig. 12. Temperature dependence of the $r_{C^{16}O^{18}O}/r_{C^{16}O_2}$ ratio for the cases of unpromoted and electropromoted Pt film under HV conditions and nanodispersed catalyst (1% Pt/YSZ) under HV and atmospheric conditions.

the region of low S_p which most likely reflects the difference in the above activation energies.

The observed decrease in S_p with temperature (Fig. 11) can explain via Eq. (16) the concomitant decrease of Λ with increasing T (Fig. 6) but also the concomitant decrease in the $r_{C^{16}O^{18}O}/r_{C^{16}O_2}$ ratio with increasing T for the case of the supported nanodispersed catalyst (Figs. 4 and 12).

The significantly smaller $r_{C^{16}O^{18}O}/r_{C^{16}O_2}$ ratio in the case of the nanodispersed catalyst (Fig. 12) is due to the occupancy of the β_2 state by lattice oxygen. As already discussed [23] this must be due to the much shorter (atomic distances) ^{16}O backspillover pathway in the case of the nanodispersed catalyst which is typically 3 orders of magnitude shorter than in the case of the supported film catalyst. Nevertheless in both cases one may conclude from the present results that the sacrificial promoter mechanism is operative both for the electropromoted Pt film and for the nanodispersed Pt/YSZ catalyst: Lattice oxygen, O(YSZ), migrates to the Pt/gas interface (β_3 state (Fig. 13a) and in the case of the nanodispersed catalyst also β_2 state (Fig. 13b)) reacts with the oxidizable species ($r_{C^{16}O_2}$), but at the same time displaces the β_1 and β_2 states to lower binding energies and thus accelerates as a promoter the rate of $C^{16}O^{18}O$ formation.

4. Conclusions

The main findings of the present work can be summarized as follows:

1. Electrochemical promotion with Pt/YSZ catalyst films can also be induced under high vacuum conditions. The measured Λ and ρ values are in general smaller than those measured for the same reaction at atmospheric pressure, apparently due to lower coverages and thus reduced importance of lateral adsorbate interactions at the same work function increase $\Delta\Phi$ [14,40,41]. Nevertheless the behavior is qualitatively the same and consistent with the recently found electrochemical promotion rules [33,40] both for the electropromoted Pt/YSZ film and for the nanodispersed Pt/YSZ catalyst.
2. The TPR rate of $C^{16}O^{18}O$ formation is directly correlated with the corresponding $^{18}O_2$ TPD spectra on the same catalyst (state β_1 and for the electropromoted film also state β_2). Also in both cases the rate of $C^{16}O_2$ formation (lattice oxygen) is directly correlated with the corresponding $^{16}O_2$ TPD spectra (state β_3 and for the nanodispersed catalyst also state β_2).
3. For both systems the presence of the β_3 state lowers both the TPD peak desorption temperature of states β_1 and β_2 and the corresponding TPR rate maximum temperatures r_{β_1} and r_{β_2}. This confirms the promotional role of the β_3 state (backspillover oxygen) which is also clearly manifested by the observed increase in $r_{C^{16}O^{18}O}$ upon the supply of backspillover ^{16}O to the catalyst surface (Figs. 3, 7, and 8).
4. Lattice backspillover oxygen (state β_3 and for the nanodispersed catalyst also state β_2) is also catalytically active ($r_{C^{16}O_2}$) and for high temperatures ($r_{C^{16}O_2} > r_{C^{16}O^{18}O}$) becomes the main reactant leading to an apparent Mars–Van Krevelen-type mechanism.
5. Observations (3) and (4) confirm the sacrificial promoter model of electrochemical promotion and metal–support interactions with O^{2-}-conducting supports. More quantitatively the model is confirmed by comparing (Fig. 10)

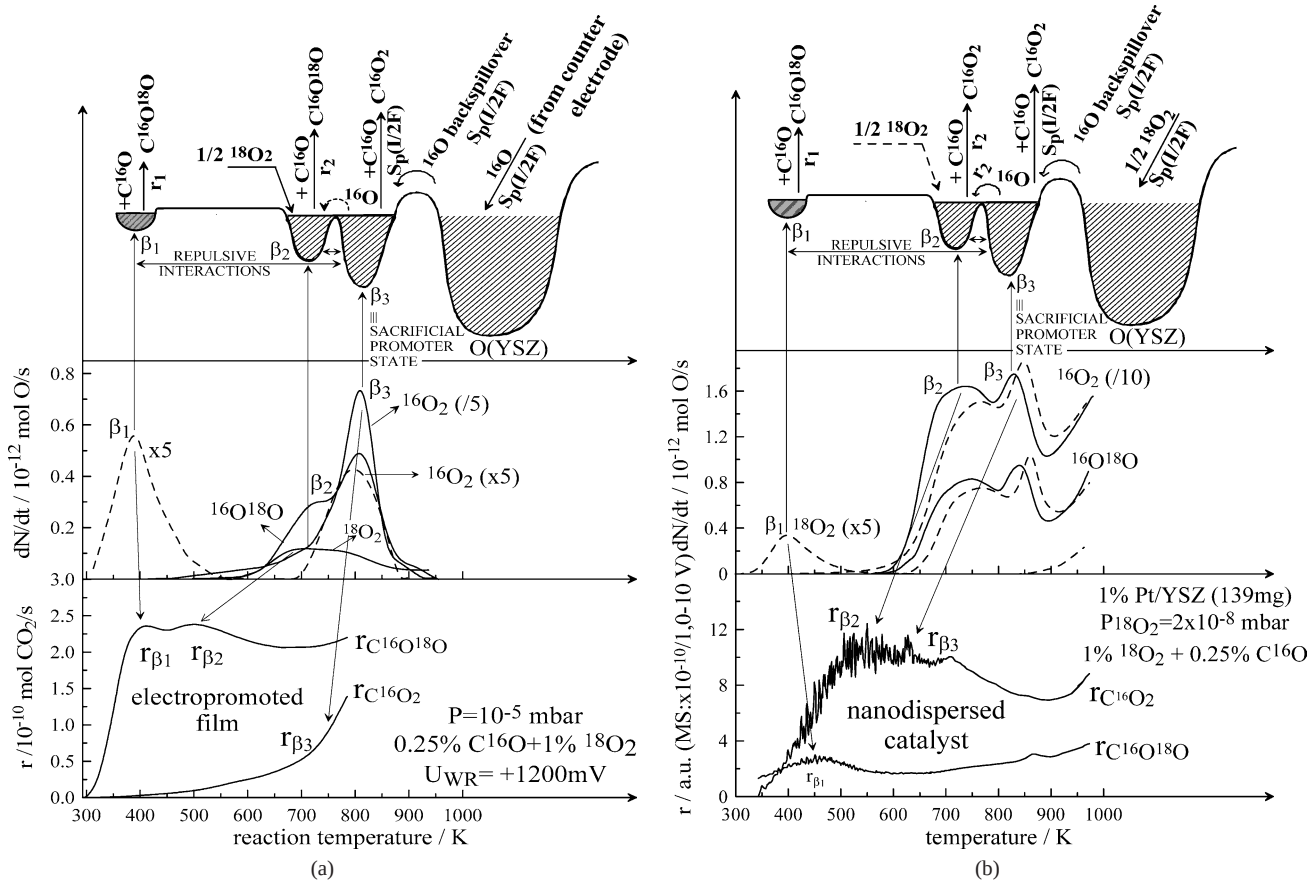

Fig. 13. (a) Sacrificial promotion mechanism for the case of CO oxidation on the electropromoted Pt film: TPR spectrum (bottom), oxygen thermal desorption spectra (middle), and energy level and population diagram of the β_1, β_2, and β_3 oxygen adsorption states (Pt surface) and of the O(YSZ) state (YSZ bulk) (top) during CO oxidation by gaseous $^{18}O_2$. Oxygen from the YSZ lattice occupies via backspillover the sacrificial promoter state β_3 ($T_P \approx 520\,^\circ$C) which reacts with adsorbed CO at a rate $S_p(I/2F)$ and at the same time promotes the rate of CO oxidation by ^{18}O occupying the β_1 and β_2 states. (b) Sacrificial promotion mechanism for the case of CO oxidation on the nanodispersed Pt catalyst (1% Pt/YSZ): TPR spectrum (bottom), oxygen thermal desorption spectra (middle), and energy level and population diagram of the β_1, β_2, and β_3 oxygen adsorption states (Pt surface) and of the O(YSZ) state (YSZ bulk) (top) during CO oxidation by gaseous $^{18}O_2$. Oxygen from the YSZ lattice occupies via backspillover the sacrificial promoter sates β_2 and β_3 which react with adsorbed CO at a rate $S_p(I/2F)$ and the same time promotes the rate of CO oxidation by ^{18}O occupying the β_1 state.

the experimental Λ ($= \Delta r/(I/2F)$) values with the $1 + \Delta r_{C^{16}O^{18}O}/\Delta r_{C^{16}O_2}$ ratio. This comparison shows clearly the validity of the sacrificial promoter model for the electrochemical promotion of Pt/YSZ films and nanodispersed Pt/YSZ catalysts.

Acknowledgments

We thank Dr. Susanne Brosda for the AC impedance characterization of the Pt/YSZ film and the EU SMART and Hellenic Secretariat of Research and Technology PENED and EPEAEK (Hellenic ministry of education) Programmes for financial support. We also thank our reviewers for helpful suggestions.

References

[1] C.G. Vayenas, S. Bebelis, S. Ladas, Nature 343 (1990) 625.
[2] J. Pritchard, Nature 343 (1990) 592.
[3] R.M. Lambert, F. Williams, A. Palermo, M.S. Tikhov, Top. Catal. 13 (2000) 91.
[4] G. Foti, S. Wodiunig, C. Comninellis, Curr. Top. Electrochem. 7 (2001) 1.
[5] C.A. Cavalca, G.L. Haller, J. Catal. 177 (1998) 389.
[6] L. Ploense, M. Salazar, B. Gurau, E.S. Smotkin, J. Am. Ceram. Soc. 119 (1997) 11550.
[7] P. Vernoux, F. Gaillard, L. Bultel, E. Siebert, M. Primet, J. Catal. 208 (2002) 412.
[8] I. Metcalfe, J. Catal. 199 (2001) 247.
[9] C. Sanchez, E. Leiva, in: W. Vielstich, H. Gasteiger, A. Lamm (Eds.), Handbook of Fuel Cells: Fundamentals, Technology and Applications, vol. 2, Wiley, Chichester, 2003.
[10] G.-Q. Lu, A. Wieckowski, Curr. Opin. Colloid Interface Sci. 5 (2000) 95.
[11] B. Grzybowska-Swierkosz, J. Haber, Annual Reports on the Progress of Chemistry, The Royal Society of Chemistry, Cambridge, 1994.
[12] J.O.M. Bockris, Z.S. Minevski, Electrochim. Acta 39 (1994) 1471.
[13] C.G. Vayenas, M.M. Jaksic, S. Bebelis, S.G. Neophytides, in: J.O.M. Bockris, B.E. Conway, R.E. White (Eds.), Modern Aspects of Electrochemistry, vol. 29, Kluwer Academic/Plenum, New York, 1996, p. 57.
[14] C.G. Vayenas, S. Bebelis, C. Pliangos, S. Brosda, D. Tsiplakides, Electrochemical Activation of Catalysis: Promotion, Electrochemical Pro-

motion and Metal–Support Interactions, Kluwer Academic/Plenum, New York, 2001.
[15] A. Wieckowski, E. Savinova, C.G. Vayenas (Eds.), Catalysis and Electrocatalysis at Nanoparticles, Dekker, New York, 2003.
[16] S. Neophytides, D. Tsiplakides, C.G. Vayenas, J. Catal. 178 (1998) 414.
[17] I. Harkness, R.M. Lambert, J. Catal. 152 (1995) 211.
[18] S. Ladas, S. Kennou, S. Bebelis, C.G. Vayenas, J. Phys. Chem. 97 (1993) 8845.
[19] C. Vayenas, D. Archonta, D. Tsiplakides, J. Electroanal. Chem. 554–555 (2003) 301.
[20] G.L. Haller, J. Catal. 216 (2003) 12.
[21] C.G. Vayenas, S. Brosda, C. Pliangos, J. Catal. 216 (2003) 487.
[22] J. Nicole, D. Tsiplakides, C. Pliangos, X.E. Verykios, C. Comninellis, C.G. Vayenas, J. Catal. 204 (2001) 23.
[23] A. Katsaounis, Z. Nikopoulou, X.E. Verykios, C.G. Vayenas, J. Catal. 222 (2004) 192.
[24] R. Imbihl, G. Ertl, Chem. Rev. 95 (1995) 697.
[25] Y.J. Mergler, A. van Aalst, J. van Delft, B.E. Nieuwenhuys, Appl. Catal. B 10 (1996) 245.
[26] P. Thormählen, M. Skoglundh, E. Fridell, B. Andersson, J. Catal. 188 (1999) 300.
[27] K. Arnby, A. Törncrona, B. Andersson, M. Skoglund, J. Catal. 221 (2004) 252.
[28] A. Bourane, D. Bianchi, J. Catal. 222 (2004) 499.
[29] V. Labalme, N. Guilhaume, E. Garhowski, M. Primet, React. Kinet. Catal. Lett. 64 (1998) 207.
[30] J.J. Lecomte, S. Haydar, D. Granger, L. Leclercq, G. Leclercq, J.P. Joly, Langmuir 19 (2003) 9266.
[31] A. Katsaounis and C.G. Vayenas, in preparation.
[32] I.V. Yentekakis, C.G. Vayenas, J. Catal. 111 (1988) 170.
[33] C.G. Vayenas, S. Brosda, C. Pliangos, J. Catal. 203 (2001) 329.
[34] I. Riess, C.G. Vayenas, Solid State Ionics 159 (2003) 313.
[35] R. Imbihl, Progr. Surf. Sci. 44 (1993) 185.
[36] R.C. Yeates, J.E. Turner, A.J. Gellman, G.A. Somorjai, Surf. Sci. 149 (1985) 175.
[37] B. Luerssen, H. Fischer, J. Janek, S. Guenther, L. Gregoratti, M. Kiskinova, in: Elletra Highlights 2002, Sincrotrone Trieste, Trieste, Italy, 2003, pp. 64–66.
[38] C.G. Vayenas, G. Pitselis, I&EC Res. 40 (2001) 4209.
[39] R. Lewis, R. Gomer, Surf. Sci. 12 (1968) 157.
[40] S. Brosda, C.G. Vayenas, J. Catal. 208 (2002) 38.
[41] G. Pacchioni, F. Illas, S. Neophytides, C.G. Vayenas, J. Phys. Chem. 100 (1996) 16653.